

Enhancement of dielectronic recombination by an electric field

Lung Ko, Victor Klimenko, and T. F. Gallagher

Department of Physics, University of Virginia, Charlottesville, Virginia 22901

(Received 3 August 1998)

Dielectronic recombination from a continuum of finite bandwidth has been examined down to very low electric fields, 60 mV/cm, with very high resolution. A tunable laser is used to excite atoms to the continuum of finite bandwidth, the broad Ba $6p_{3/2}11d$ autoionizing state, which straddles the Ba⁺ $6p_{1/2}$ limit. Atoms which make transitions into the high-lying Ba $6p_{1/2}nd$ states and radiatively decay to the bound $6snd$ states are detected by field ionization. The recombination, integrated over energy, has been measured for fields from 60 mV/cm to 28 V/cm, showing a peak at 0.5 V/cm, in agreement with expectation based on calculations done for other systems. The final-state distribution has been measured, showing that the outer electron remains a spectator in the radiative decay. At fields below 1.0 V/cm and binding energies less than 12 cm^{-1} below the Ba⁺ $6p_{1/2}$ limit we find a deviation of our experimental results from the isolated resonance approximation. [S1050-2947(99)03803-2]

PACS number(s): 32.80.Rm, 32.80.Dz, 34.80.-i

I. INTRODUCTION

Dielectronic recombination (DR) is an important mechanism for the recombination of ions and electrons in high-temperature plasmas. However, measuring it in a clean quantitative way is a challenge. The first merged and crossed beam measurements [1,2], were heroic efforts. Electron-beam ion sources and electron beam ion traps made it vastly easier to measure DR, and storage rings, with cold ions, have made possible an unprecedented energy resolution, 0.01 eV, in measurements of DR [3].

One drawback of all these approaches to measuring DR is that electric and magnetic fields are unavoidable, because beams must be merged and products separated. As a result there are always fields present. The effects of fields have long been appreciated, and it is possible to take them into account in calculating DR rates. However, there have been no measurements of DR in zero field, and there remain some uncertainties about field effects.

Here we report measurements of DR from a continuum of finite bandwidth in Ba. We have made measurements from 60 mV/cm to 28 V/cm to address the above questions. Using the high resolution (0.2 cm^{-1}) of our approach, we have also measured the final bound-state distribution after DR, confirming one of the usual assumptions made in calculations. Finally, our data show the breakdown of the isolated resonance approximation when its limits of validity are reached.

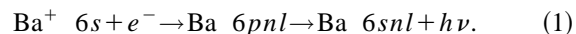
This paper is organized in the following manner. In Sec. II we outline a model of DR from a continuum of finite bandwidth. Section III is a description of the experimental approach. In Sec. IV we present and discuss our results, and Sec. V is our conclusion.

II. MODEL FOR DIELECTRONIC RECOMBINATION FROM A CONTINUUM OF FINITE BANDWIDTH IN AN ELECTRIC FIELD

The model for DR through a continuum of finite bandwidth we adopt in this work is basically the same as the one

used in an earlier paper (from now on referred to as SLG) by Story, Lyons, and Gallagher [4] and therefore we shall only state the key points here.

Dielectronic recombination between a free electron and a ground state Ba⁺ ion can occur through the process:



The first step of the process, the capture, is simply the inverse of the autoionization process $\text{Ba } 6pnl \rightarrow \text{Ba}^+ 6s + e^-$, and therefore by the principle of detailed balance may be characterized by the autoionization rate $\Gamma_s(nl)$, where the subscript s refers to the Ba⁺ $6s$ continuum. After the capture, the electron in the Ba $6pnl$ state may either decay back into the Ba⁺ $6s$ continuum, at the rate $\Gamma_s(nl)$, or into the Ba⁺ $5d$ continuum, at the rate $\Gamma_d(nl)$, or remain in the nl orbital while the core electron undergoes radiative stabilization, $\text{Ba}^+ 6p \rightarrow \text{Ba}^+ 6s$, at a rate A . Note that the captured electron remains a spectator in last step. A is therefore a constant irrespective of the values of n and l . The contribution to DR from the process in Eq. (1) is therefore

$$S(nl) \propto \Gamma_s(nl) \frac{A}{\Gamma_s(nl) + \Gamma_d(nl) + A}. \quad (2)$$

The autoionization rates follow the well-known scaling $\Gamma_s(nl) = \gamma_s(l)n^{-3}$ and $\Gamma_d(nl) = \gamma_d(l)n^{-3}$. Both $\gamma_s(l)$ and $\gamma_d(l)$ are rapidly decreasing functions of l [5]. The total DR rate S is obviously given by multiplying Eq. (2) by the degeneracy factor $2l+1$ and summing over all values of n and l . As discussed by SLG, the summation yields

$$S \propto \frac{3}{2} NA, \quad (3)$$

where N is the number of states for which $\Gamma_s(nl) + \Gamma_d(nl) > A$.

Although Eq. (3) pertains to DR in zero field, it suggests that if one can increase the number of states for which the autoionization rate exceeds the core fluorescence rate, one

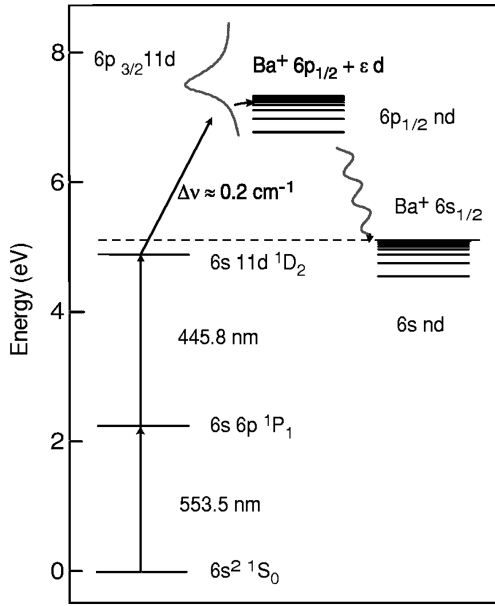


FIG. 1. Scheme for laser excitation to the $6p_{3/2}11d$ autoionizing state using the isolated core excitation technique. The step that is analogous to the dielectronic capture of an electron by an ion takes place when internal conversion $6p_{3/2}11d \rightarrow 6p_{1/2}nd$ occurs, and the core radiatively decays: $\text{Ba}^+ 6p_{1/2} \rightarrow \text{Ba}^+ 6s$.

can enhance the total amount of DR. In fact, this can be accomplished by application of an external field, and is the mechanism for DR enhancement in any external field, regardless of whether the field is electric or magnetic. The essential idea is as follows. Since autoionization rates decrease very rapidly with l , in zero field many high- l states have autoionization rates less than the radiative decay rate and do not contribute to DR. When a field is present l is no longer a good quantum number, and the nl zero-field states are converted to nk Stark states, which are linear superpositions of the nl states. To a first approximation the autoionization rates of the nk Stark states are equal to the average of the autoionization rates of the zero-field nl states. In essence, the high autoionization rates of the low- l states, ten orders of magnitude in excess of the radiative decay rate, are redistributed over all the nk Stark states, thus increasing the number of states for which the autoionization rate exceeds the fluorescence rate, leading to enhanced DR. On the other hand, the external electric field can also field ionize the stabilized states which lie above the classical field ionization threshold, thus contributing negatively to DR. The rate equation for DR in an external electric field has a form similar to Eq. (2):

$$S_E(nk) \propto \Gamma_s(nk) \frac{A}{\Gamma_s(nk) + \Gamma_d(nk) + A}. \quad (4)$$

In this work we have studied the enhancement of DR from a continuum of finite bandwidth (CFB) [6] instead of a true continuum. The CFB is the broad $6p_{3/2}11d$ autoionizing state which straddles the $6p_{1/2}$ limit with its tail extending below the $\text{Ba}^+ 6p_{1/2}$ limit, as shown by the energy-level diagram of Fig. 1. In this region configuration interaction couples the broad autoionizing state to the $6p_{1/2}nd$ states. Atoms excited to the $6p_{3/2}11d$ state may undergo an internal

conversion process, in which the core undergoes a quadrupole transition upon colliding with the outer electron, $6p_{3/2}11d \rightarrow 6p_{1/2}nd$. This process mimics the capture step in true DR. After the capture into the $6p_{1/2}nd$ state, the atom may either autoionize to the $\text{Ba}^+ 5d$ or $\text{Ba}^+ 6s$ continua, revert back to the CFB, or undergo stabilization. Thus, DR from a CFB is completely analogous to true DR, and the corresponding rate equation is therefore

$$S(nd) \propto R(nd) \frac{A}{R(nd) + \Gamma(nd) + A}, \quad (5)$$

where $\Gamma(nd)$ is the sum of decay rates into the real continua, $R(nd) = rn^{-3}$, and $\Gamma(nd) = \gamma n^{-3}$. In an external electric field, the obvious analog of Eq. (4) is

$$S_E(nk) \propto R(nk) \frac{A}{R(nk) + \Gamma(nk) + A}, \quad (6)$$

where $R(nk)$ is the $6p_{3/2}11d \rightarrow 6p_{1/2}nd$ transition rate spread over all the $6p_{1/2}nk$ states. Since the $6p_{3/2}11d$ state is unaffected by the electric field we applied, it is coupled only to the $6p_{1/2}nd$ component of the Stark states, and therefore $R(nk) = rn^{-4}$. Similarly, $\Gamma(nk) = \gamma_E n^{-4}$, where γ_E is related to $\gamma(l)$ as follows [7,8]:

$$\gamma_E = \sum_{l=0}^{n-1} \gamma(l). \quad (7)$$

The quantity we measured in this experiment was the population of stabilized states as a function of n , or equivalently as a function of their energies, and the measurements were compared to our model for DR from a CFB as follows. For zero electric field ($E=0$), we compared the data to Eq. (5) recast in terms of DR rate per unit energy (W) of the stabilized states. Specifically, using $W = -0.5n^{-2}$, we reexpress Eq. (5) as

$$\frac{dS_0}{dW} \propto \frac{rA}{(-2W)^{3/2}(r+\gamma)+A}, \quad (8)$$

where the subscript 0 refers to the fact that $E=0$. Similarly, Eq. (6) is rewritten as

$$\frac{dS_E}{dW} \propto \frac{rA}{(-2W)^2(r+\gamma_E)+A}. \quad (9)$$

For Ba, in atomic units, $A = 3.88 \times 10^{-9}$ [9], $r = 0.05$, $\gamma = 0.05$ [7,10,11], and $\gamma_E = 0.53$ [12].

As a matter of experimental approach, DR from a continuum of finite bandwidth differs from true DR in one respect. In Eqs. (8) and (9) we assume an even distribution of the number of incoming electrons from the CFB for all binding energies. Stated another way, we have assumed that for our region of interest, below the $\text{Ba}^+ 6p_{1/2}$ limit where the $6p_{3/2}11d$ and $6p_{1/2}nd$ states interact, the laser excitation strength to the CFB is constant. This, however, is not the case. Figure 2 shows an excitation spectrum of the $6p_{3/2}11d$ state in this region. From the figure, it is clear that superimposed on the slowly varying envelope of the $6p_{3/2}11d$ state are two series of peaks. The larger series of peaks reflects the

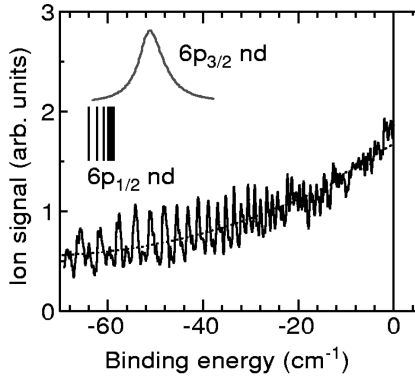


FIG. 2. Excitation profile of the $6p_{3/2}11d$ state relative to the $\text{Ba}^{+} 6p_{1/2}$ threshold. Solid line: experimental spectrum obtained by collecting all ions formed. Dotted line: average excitation for normalization.

presence of channel interaction with the $6p_{1/2}nd$ states, while the smaller series comes from interaction with the $6p_{1/2}ns$ states.

The slowly rising profile of the $6p_{3/2}11d$ state, as opposed to a true continuum, mandates a slight modification of the rate equations given above. That is, one needs to take into account the varying number of atoms excited to the CFB in different parts of the $6p_{3/2}11d$ excitation spectrum. Thus Eqs. (8) and (9) should be multiplied by a weighting factor proportional to the profile f of the CFB:

$$\frac{dS_{E,0}}{dW} \rightarrow \frac{dS_{E,0}}{dW} f. \quad (10)$$

The line-shape function f is approximately Lorentzian and has been thoroughly studied using the isolated core excitation technique [7,8,13–15,10,16] In comparing our data to the model, we found it more convenient to normalize our measured recombination signals by dividing them by the measured line shape of the CFB such as the one shown by the broken line in Fig. 2 before comparing them to Eqs. (8) and (9).

III. EXPERIMENTAL APPROACH

The objective of the experiment was to excite barium atoms to the broad $6p_{3/2}11d$ autoionizing state, which served as the continuum of finite bandwidth, and measure the number of atoms which underwent radiative stabilization and ended up in bound $6snd$ Rydberg states. The broad $6p_{3/2}11d$ autoionizing state was prepared using the isolated core excitation approach, as shown in Fig. 1. Barium atoms were excited sequentially by three nanosecond Littman dye lasers which were pumped by the second and third harmonics of a Q -switched Nd:YAG (yttrium aluminum garnet) laser. The first two lasers, which overlapped in space and time, excited the atoms to the $6s11d \ ^1D_2$ state. Approximately 10 ns later, the third laser arrived and drove the $\text{Ba}^{+} 6s_{1/2}$ to $6p_{3/2}$ transition near 455.3 nm. The linewidth of the third laser was kept between 0.2 and 0.4 cm^{-1} . The atomic source was a thermal beam of barium atoms which effused from a resistively heated oven. The three lasers crossed the atomic beam at slight angles between a pair of capacitor plates spaced by

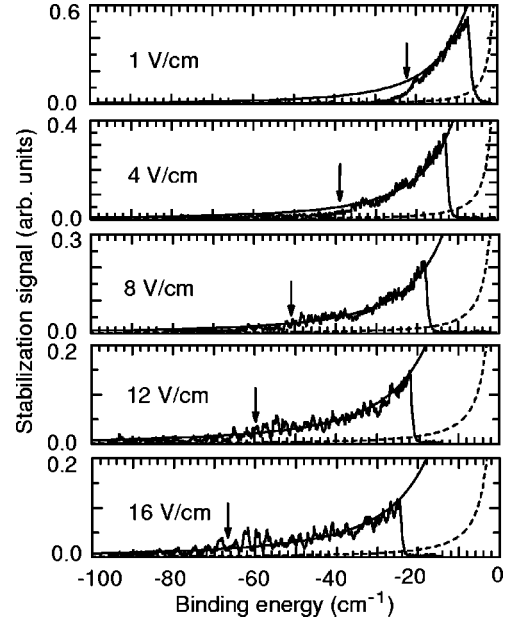


FIG. 3. Simulated DR signals vs static field. The arrows indicate the Inglis-Teller limits. Solid curve: calculated signal level for complete Stark mixing. Dashed curve: calculated signal level for zero field.

1.27 cm. Polarization of the lasers was typically along the direction of the electric field, but for a subset of the data presented below they were circularly polarized in the same sense. Approximately 200 ns after the laser excitation, a field pulse was applied to the bottom plate to accelerate either electrons or ions upward through a group of holes in the top plate and into a microchannel-plate detector situated ~ 2 cm above the top plate. The field ionization signal from the detector was then gated and integrated by a boxcar integrator before being digitized and recorded on a personal computer. The data consisted of the field ionization signal recorded as the frequency of the third laser was continuously tuned by a synchronous motor over many shots of the laser. The excitation and data acquisition process was repeated at the 20 Hz repetition rate of the Nd:YAG laser.

IV. RESULTS AND DISCUSSION

A. Dielectronic recombination vs static fields

By scanning the third laser in the region below the $\text{Ba}^{+} 6p_{1/2}$ limit and collecting the field-ionized electrons, we obtained stabilization signals (or simulated DR signals) versus the binding energies of the $6p_{1/2}nd$ states for various static fields, as shown in Figs. 3 and 4. In these figures, the noisy traces are the data, the solid smooth curve is the calculated signal level given by Eq. (6) for the case of complete Stark mixing, and the dashed smooth curve is the calculated signal level for zero field according to Eq. (5). Let us first focus on Fig. 3. In these traces two features are particularly noteworthy. First, for a given static field E , there is a sharp cutoff in the stabilization signal at the position given by the classical field ionization threshold $W_C = -2E^{1/2}$. Second, the bulk of the stabilization signal is concentrated between the field ionization limit and the Inglis-Teller limit, which is indicated by an arrow. (The Inglis-Teller limit is the binding

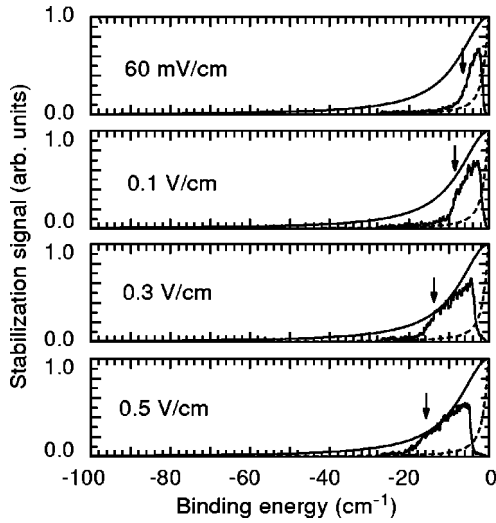


FIG. 4. Simulated DR signals vs static field. The arrows indicate the Inglis-Teller limits. Solid curve: calculated signal level for complete Stark mixing. Dashed curve: calculated signal level for zero field.

energy at which the Stark manifolds of adjacent n 's begin to intersect, and we shall assume in a model calculation given below that for states lying above this limit Stark mixing is complete.) This constitutes an incontrovertible manifestation of the enhancement of DR by way of character mixing among the high- l and low- l zero-field states. In these traces, we also note the curious hump-shaped structures in the vicinity of the Inglis-Teller limits. In the bottom two traces of the figure, these structures are quite distinct. Clearly, our simple model is inadequate to accommodate these local structures. Nevertheless, the overall agreement between the data and the model is good. Just below the field ionization limit, the signal reaches the calculated Stark-mixed level, and below the Inglis-Teller limit, the signal eventually drops to nearly zero.

In Fig. 4, we show the stabilization signals for various fields below 1.0 V/cm. The presence of stray fields at the interaction region prevented us from measuring the stabilization signal in strictly zero field. For the top trace in the figure, the nominal field value of 60 mV/cm was estimated from the location of the midpoint of the field ionization edge using the classical field ionization formula $W_c = -2E^{1/2}$. The stray fields originated at least in part from the ambient plasma of ions formed as a product of autoionization. There is a hint of a departure of the data from the calculation in the 1.0-V/cm trace of Fig. 3, but, in Fig. 4, one finds unambiguous departure of the measured signals from the model calculation. While the Inglis-Teller limit moves to higher energy with decreasing field, as expected, the stabilization signals above the Inglis-Teller limits fall below that given by the isolated resonance approximation. In Fig. 4, this phenomenon becomes increasingly distinct as the static field decreases. Due to signal fluctuations, there is some uncertainty in determining at exactly what binding energy the data deviate from the curve, save for the fact that the deviation begins in the neighborhood of -12 cm^{-1} . We further note that the stabilization signals do not differ from the model curve merely by a constant factor or offset, but rather by their general shapes.

Various reasons could be responsible for the difference between the measured and calculated stabilization signals. The reduction in the experimental signal might be an experimental artifact. A possible effect which would lead to the sort of reduction we have observed is collisional ionization of the high Rydberg states by the background ions and neutrals at the interaction region. By ionizing the stabilized Rydberg states with a fast field pulse (10-ns rise time), and varying the time delay between laser excitation and the field pulse, we could determine the effects of collisions. However, we have found no significant change in the field electron signal for delays ranging from 100 to 600 ns. We have therefore ruled out the effect of collisional ionization. We have also ruled out the possibility of photoionization of the stabilized states by the third laser via the $\text{Ba}^+ 6s \rightarrow 6p_j$ transitions. Since the $\text{Ba}^+ 6p_{1/2}$ level is approximately 2000 cm^{-1} below the $\text{Ba}^+ 6p_{3/2}$ level, photoionization through the $\text{Ba}^+ 6s \rightarrow 6p_{1/2}$ transition is out of the question. On the other hand, based on the fact that the profile of the amplified spontaneous emission (ASE) of the third laser was centered at more than 200 cm^{-1} below the $\text{Ba}^+ 6s \rightarrow 6p_{3/2}$ transition frequency, and that the laser was not focused at the interaction region, we believe that ASE had no material effect on our data. We believe that the experimental curves of Fig. 4 are correct, so we must examine the model. Varying the parameters of the model r , γ_E , γ , and A obviously will not lead to better agreement between the model curve and the data, since they differ in their general shapes. Based on these considerations, we believe that our data indicate the breakdown of our model for DR near the $\text{Ba}^+ 6p_{1/2}$ threshold. This possibility will be discussed in Sec. IV C.

From Eqs. (8) and (9), we can evaluate the amounts (up to a constant factor) of simulated DR at various field strengths. Above the Inglis-Teller limit defined by $W_l = -0.5(3E)^{2/5}$, Eq. (9) holds. For the sake of simplicity, we shall assume that Eq. (8) prevails below the Inglis-Teller limit. The total simulated DR at a given field is then given by integrating dS_E/dW over energy:

$$S_E = \int_{-\infty}^{W_l} \frac{rA}{(-2W)^{3/2}(r+\gamma)+A} dW + \int_{W_l}^{W_c} \frac{rA}{(-2W)^2(r+\gamma_E)+A} dW. \quad (11)$$

The results of the calculation are compared to our measurements in Fig. 5. In this figure the data are normalized to the point at 8.0 V/cm. The agreement between the data and calculation is reasonably good. The error bars reflect signal fluctuations due to thermal instability of the oven and the power fluctuations of the lasers. It is interesting to note that our data indicate a maximum enhancement factor of approximately 2 at an electric field of about 0.5 V/cm. This is to be compared to a calculation for Mg [17], giving enhancement factors of 2.9, 2.4, 2.1, and 1.5, at 1, 5, 20, and 100 V/cm, respectively.

We now examine the stabilization signal in greater detail. Figures 6(a) and 6(b) show high-resolution scans of the third laser in zero electric field, with all three lasers circularly and linearly polarized, respectively. The solid traces are the field

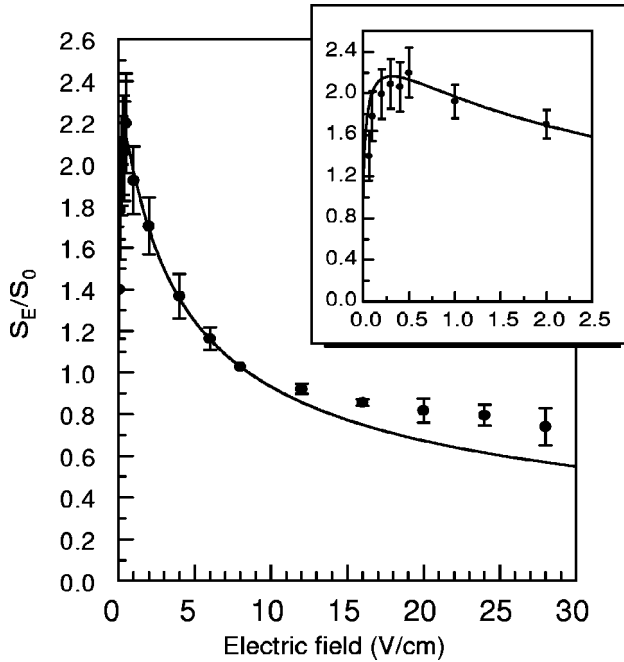


FIG. 5. Enhancement of simulated DR vs static field. The solid curve is the calculated enhancement. The 8.0-V/cm DR yield is used to normalize the data.

ionization signals of the stabilized states, and the dashed traces are the autoionization signals. Since the autoionized electrons arrived at the detector ~ 50 ns after the laser pulses, their signal was well separated in time from the field ionization signal. The two signals were recorded simultaneously as the wavelength of the third laser was scanned. Note that the autoionization electron signals have been scaled down to fit in the figures. In reality they were typically 200 times larger than the field ionization electron signals in this region. Thus

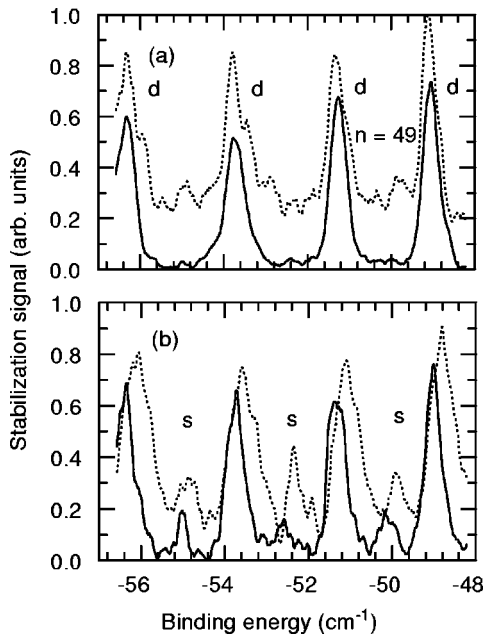


FIG. 6. Stabilization signal (solid trace) vs autoionization signal (dashed trace). (a) Circular polarization. (b) Linear polarization. The letter *d* denotes features due to the $6p_{1/2}nd$ states, and *s* denotes features due to the $6p_{1/2}ns$ states.

TABLE I. Relevant collision channels for the spectral analysis.

$J=1$	$J=3$
$6p_{3/2}nd_{5/2,3/2}$	$6p_{3/2}nd_{5/2,3/2}$
$6p_{1/2}nd_{3/2}$	$6p_{1/2}nd_{3/2}$
$6p_{1/2}ns_{1/2}$	
Continua	Continua

the autoionization electron signals reflect the profiles of total excitation, as would be obtained by detecting ions. Figure 6(a), obtained with circularly polarized excitation, is due to $J=3$ states. The peaks in both spectra are due to the $(6p_{1/2}nd)_{J=3}$ states, and it is perhaps not completely surprising that they occur at the same energies. The situation is clearly different in Fig. 6(b), obtained with linear polarization, which contains both the $J=1$ and channels. In Fig. 6(b), several features stand out upon casual inspection. First, not only the $6p_{1/2}nd$ states but also $6p_{1/2}ns$ states appear in both the autoionization and the stabilization signals. Furthermore, unlike Fig. 6(a) the autoionization and stabilization signals are quite different. Let us focus first on the features associated with the $6p_{1/2}nd$ states, marked as *d* in Fig. 6. The autoionization signal is broader and shifted to higher energy relative to the stabilization, or field ionization, signal. The latter is essentially the same as in Fig. 6(a). The features associated with the *ns* states, marked as *s* in Fig. 6(b), are even more surprising. The field ionization signal is approximately at the minimum of the autoionization signal. A final important aspect of Figs. 6(a) and (b) is that the autoionization signals do not go to zero anywhere but have significant apparent backgrounds.

To understand the spectra of Fig. 6 we need to consider the origin of the two different spectra, and we begin with the wavefunction for the autoionizing states. To facilitate our discussion, in Table I we list the collision channels involved in our problem. Let us consider the $J=3$ states relevant to Fig. 6(a) first. For a given energy, the atomic wave function may be written as

$$\Psi_{J=3} = Z_1 |6p_{3/2}nd_j\rangle_{J=3} + Z_2 |6p_{1/2}nd_{5/2}\rangle_{J=3} + |\text{continua}\rangle_{J=3}, \quad (12)$$

where Z_1^2 and Z_2^2 are spectral densities of the respective channels and depend strongly on the energy. We have ignored the $6p_{1/2}ng_j$ states, for they are not coupled to the $6p_{1/2}nd_j$ states [15]. For simplicity the continuum channels are denoted collectively by one ket state. Throughout this paper, the fine structure of the outer electron will be specified only for labeling purposes. Our experimental data do not resolve these fine structures. The laser excitation probability is given by the autoionization signal S_{AI} , which is expressed as simply

$$S_{AI} \propto Z_1^2, \quad (13)$$

since the variation of the overlap integral of the $6s_{1/2}11d \rightarrow 6p_{3/2}11d$ transition is negligible over this energy interval [16]. The excitation spectrum of the $6p_{3/2}11d$ state is given by Z_1^2 , and Fig. 2 is the $J=1$ analog of Z_1^2 . Above the $6p_{1/2}$

limit Z_1^2 is approximately Lorentzian, but below the limit it is structured by the interaction with the $6p_{1/2}nd$ states. The transition of the excited atoms undergoing the internal conversion $6p_{3/2}nd \rightarrow 6p_{1/2}nd$ is proportional to Z_2^2 , and it follows that the recombination signal S_{RC} is given by the product $Z_1^2 Z_2^2$, i.e.,

$$S_{RC} \propto Z_1^2 Z_2^2. \quad (14)$$

Thus from Fig. 6(a) one infers that the maxima in Z_1^2 and Z_2^2 are coincident on the energy scale. On the basis of Eqs. (13) and (14) we expect the recombination signal to be narrower than the autoionization signal. However, we are at the limit of our spectral resolution and both signals of Fig. 6(a) have the same widths.

To discuss the combined $J=1$ and $J=3$ spectra of Fig. 6(b) we begin with the $J=1$ analog of Eq. (12),

$$\begin{aligned} \Psi_{J=1} = & Z_1 |6p_{3/2}nd_j\rangle_{J=1} + Z_2 |6p_{1/2}nd_{j'}\rangle_{J=1} \\ & + Z_3 |6p_{1/2}ns_{1/2}\rangle_{J=1} + |\text{continua}\rangle_{J=1}. \end{aligned} \quad (15)$$

Let us first concentrate on the nd features of Fig. 6(b). Previous measurements [12] have shown that, away from perturbing $6p_{3/2}nd$ states, the $6p_{1/2}nd$ $J=1$ and 3 states have the same widths, showing that both interact equally strongly with continua above the $5d$ and $6s$ limits. Thus the excess widths of the d states in the autoionized electron signal are probably due to stronger coupling between the $(6p_{1/2}nd_{j'})_{J=1}$ states and the $(6p_{3/2}nd_j)_{J=1}$ state, either directly or via the continua. As a result, the peak in Z_1^2 is wider for $J=1$ than for $J=3$. Nonetheless, the peak in Z_2^2 for $J=3$ is still narrower than our laser resolution, for the recombination signal associated with the $6p_{1/2}nd$ states appears to be the same for $J=1$ and 3.

Turning our attention to the ns features of Fig. 6(b), we find a more surprising result. The features in the stabilization signal are aligned with minima in the autoionization signals. The misalignment can only occur if there are multiple interacting continua in our problem. If there was only one continuum the autoionization signal Z_1^2 would go to zero, at the minima, and the stabilization signal $Z_1^2 Z_2^2$ would vanish at that point, unlike what we have observed.

B. Final-state distribution

In the model given in Sec. II, it is assumed that $6p_{1/2}nd$ states contribute to stabilization through the process $6p_{1/2}nd \rightarrow 6sn'd + h\nu$, with $n' = n$. In other words, the outer electron remains a spectator when the core radiatively decays. This assumption is always used in the isolated resonance approximation, and it has been invoked in most theoretical calculations on DR [18–20]. During the past two decades numerous experiments have been performed to study the inverse process $6snd + h\nu \rightarrow 6p_{1/2}n'd$ using the isolated core excitation technique [7,8,13–15,10,16]. It was shown that in the shake-up process $6snd \rightarrow 6p_{1/2}n'd$ transitions to states with $n' \neq n$ were possible. By the same token, the stabilization process is in principle not restricted to states with $n' = n$. As we have already noted, the total stabilization signal via a $6p_{1/2}nd$ state is given by $Z_1^2 Z_2^2$. The branching ratio to final $6snd$ states is given by the ratios of the squared

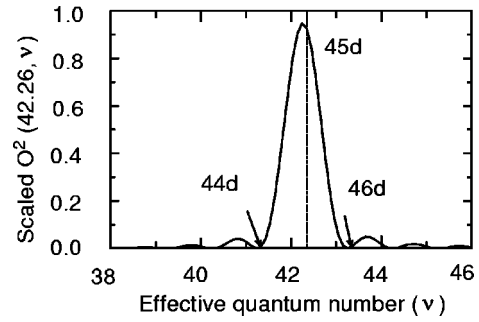


FIG. 7. $O^2(\nu, \nu')$ vs the effective quantum number of the $6snd$ states for an initial $6p_{1/2}45d$, for which $\nu' = 42.26$. The amplitude of the graph is the actual amplitude divided by 6×10^9 . The arrows indicate the positions of the $6snd$ states.

dipole matrix elements connecting them to an initial $6p_{1/2}nd$ state. For an initial $6p_{1/2}nd$ state with effective quantum number ν' , the squared matrix element connecting it to a $6snd$ state with effective quantum number ν is given by [16]

$$|D|^2 = Z_2^2(\nu') |\langle 6s\nu d | r | 6p\nu' d \rangle|^2 = \mu^2 Z_1^2(\nu') O^2(\nu d, \nu' d), \quad (16)$$

where $\mu^2 = |\langle 6s | r | 6p \rangle|^2$, and $O(\nu d, \nu' d)$ is the overlap integral given by

$$O(\nu, \nu') \cong \frac{2\nu'^2 \nu^2 \sin[\pi(\nu - \nu')]}{\nu + \nu' \pi(\nu - \nu')}. \quad (17)$$

We normalize the wave functions per unit energy so that $O^2(\nu d, \nu d) = \nu^3$, for example. Figure 7 shows a scaled graph of the overlap integral squared, for $\nu' = 42.26$, corresponding to the peak of the $6p_{1/2}45d$ state with quantum defect 2.74 [10]. Since the overlap integral is proportional to a sinc function, it vanishes at $\nu = \nu' + i$, where i is a nonzero integer. For a fixed wavelength of the third laser, ν' is a constant, and so the relative amounts of stabilized population in the satellite states, i.e., the neighboring states of the $6s45d$ state, are given entirely by $O^2(42.26, \nu)$. Given that the quantum defect of the $6snd$ series is 2.68, the bound satellite states are located near the zeros of $O^2(42.26, \nu)$. As such, the graph shows that the stabilized populations in the nearest satellite states are two orders of magnitude smaller than the population in the $6s45d$ state.

To determine experimentally how much the satellite states, i.e., those with $\nu \neq \nu'$, contributed to DR, we used the time-resolved pulsed field ionization technique. A slow pulse of 3- μ s rise time was used to field ionize the bound states when the third laser (circularly polarized) was set to excite three neighboring $6p_{1/2}nd$ states, as shown in the inset of Fig. 8. The three traces in the main graph are oscilloscope signals. The slow falling edges in these traces are probably due to the kinematics of the field ionization process. With the background noise level taken into account, the successive traces show no subsidiary peaks coincident in time with the main features of the adjacent states. For instance, any significant amount of population in the nearest higher-lying satellite state around state B would manifest itself in the dashed trace as a subsidiary peak coincident in time with peak C in the upper trace. The lack of such features suggests that sta-

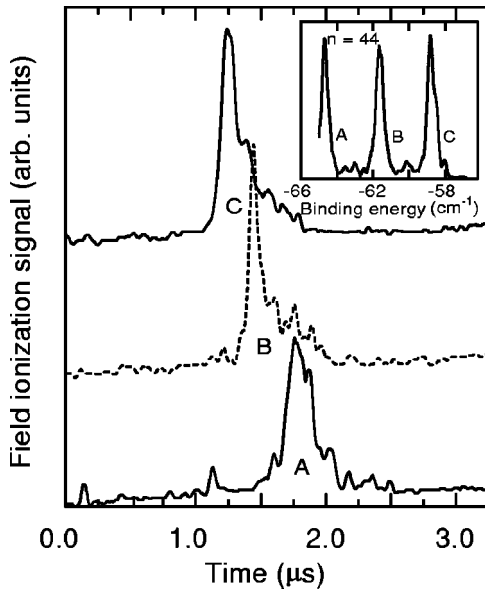


FIG. 8. Time-resolved field ionization signals. When the third laser is tuned to the $6p_{1/2}44d$, $6p_{1/2}45d$, and $6p_{1/2}46d$ states, labeled in the inset by A, B, and C, we obtain the field ionization traces labeled A, B, and C in the main figure. Since the ionization field is applied as a ramp rising over $3 \mu\text{s}$, the higher-lying $6s46d$ state, labeled C, ionizes earliest. It is clear that each of the three $6p_{1/2}nd$ states leads to a different final $6snd$ state, presumably the one in which the outer d orbit is unchanged. All three field ionization traces have sharp rising and slow falling edges due to the kinematics of the field ionization process.

bilization into satellite states is totally insignificant, in accordance with the assumption made in the isolated resonance approximation. To ensure that the same holds in DR through Stark states, we have repeated the measurements in the presence of a static electric field. Figure 9 shows stabilization signals at 0, 20, and 40 V/cm. The third laser was tuned to points (B,C), (B',C'), and (B'',C''), and the correspond-

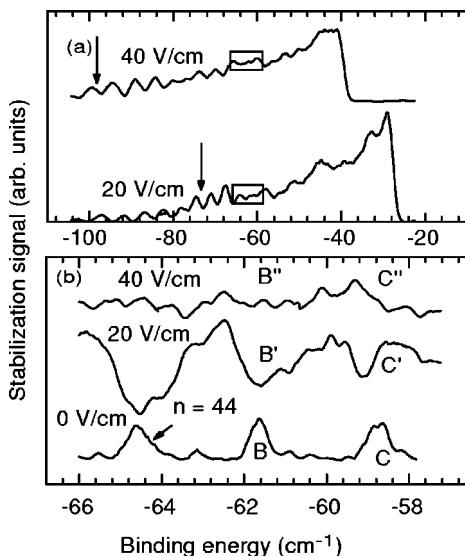


FIG. 9. Stabilized population vs the electric field. (a) Arrows indicate the Inglis-Teller limits. (b) Higher-resolution scans of the boxed areas in (a). An enlarged zero-field scan is included for comparison.

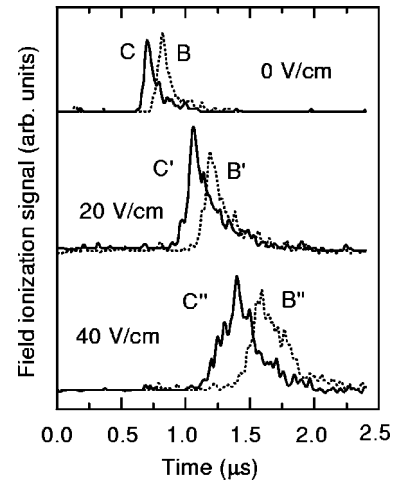


FIG. 10. Time-resolved field ionization signals observed when exciting to the $6p_{1/2}$ Rydberg states at points B, C, B', C', B'', and C'' in Fig. 9. As shown, the static fields are 0, 20, and 40 V/cm. With or without the static field, exciting different $6p_{1/2}$ Rydberg states leads to different final $6s$ Rydberg states, presumably ones in which the outer electron's orbit has not changed during the radiative decay. The shift to later times with increasing static field does not mean that a higher ionization field is required but is a kinematic artifact.

ing field ionization signals of the oscilloscope are shown in Fig. 10. In this figure, for $E \neq 0$, each signal contains a band of Stark states, since the laser linewidth was much wider than the spacings between adjacent Stark states. The overall shift of the of the signals to later times with increasing field strength is due to the fact that the static field was applied in the direction opposite to that of the field pulse. Thus at higher fields longer times elapsed before the field pulse was large enough to ionize the bound states. Additionally, the separation between and widths of each pair of traces increased with the static field strength. This is related to the temporal shape of the field pulse, which rose to a maximum value before decreasing. With increasing static field strength, the atoms were ionized closer to the maximum of the field pulse, where it rose more slowly. In any event, the data show no evidence of stabilization to satellite Stark states. Thus the assumption that the excited ionic core decays while the outer electron remains a spectator is fulfilled even if a field is present.

C. Limitations of the isolated resonance approximation

The model of DR presented earlier is both simple and intuitively plausible. However, its validity is questionable in the following situations: (a) when the autoionization rates become comparable to the radiative rate of the core ($\Gamma \approx A$), and (b) when the autoionizing resonances begin to overlap. It is instructive to see how these two limitations would emerge in the DR via Ba $6pnl$ states in zero field. Let us first consider case (a). The validity of a rate equation such as Eq. (2) is based on the principle of detailed balance. In the present context, the capture process is envisioned as the inverse of autoionization, whose rates scale as $1/n^3$. However, this implicitly assumes that during the capture the only decay channel for the intermediate Ba $6pnl$ states is

autoionization to the continua, and the radiative decay of the core is a slow process. Thus the loss of particle flux from the subspace (in the sense of the Hilbert space) of the doubly excited states to the singly excited bound states by coupling to the radiation field is neglected. In other words, the capture and the core fluorescence are regarded as two independent processes. This assumption is valid when $\Gamma \gg A$, but not for $\Gamma \leq A$, which is eventually realized as $n \rightarrow \infty$. Conversely, we expect the autoionization rates of the doubly excited states to deviate from γ/n^3 when $\Gamma \leq A$. Since $\Gamma = \gamma n^{-3}$ the limit of validity is $n = (\gamma/A)^{1/3}$.

Now let us consider case (b). The isolated resonance approximation simply states that each doubly excited state contributes to DR independently of other states, and that the total DR is the sum of all such individual contributions. This is a reasonable approximation as long as the doubly excited states are well resolved, and the resonances do not overlap. If the resonances overlap applying the isolated resonance approximation seems to introduce multiple counting. Irrespective of their autoionization rates, the Ba $6pnl$ states are certain to overlap when $A = 1/n^3$, which is a higher value of n than is required to reach the limit of validity in case (a).

In the presence of an electric field, the limits of validity due to cases (a) and (b) are $n = (\gamma_E/A)^{1/4}$ and $n = 1/A^{1/4}$, respectively. They are reached at essentially the same value

of n since $\gamma_E = 0.53$. Setting $n = (\gamma_E/A)^{1/4}$ yields $n = 109$, or a binding energy of 10 cm^{-1} . This energy coincides almost perfectly with the energy at which the experimental and calculated curves of Fig. 4 diverge. Consequently, we take the data of Fig. 4 to be a demonstration of the failure of the isolated resonance approximation.

V. CONCLUSION

These measurements have shown that DR rate reaches its maximum value, twice the zero-field rate, at the very low field of 0.5 V/cm. This finding is in accord with calculations done for Mg [17], and with a simple model developed using the isolated resonance approximation, at least for fields in excess of 1.0 V/cm. At lower fields, we find a deviation of our experimental results from the isolated resonance approximation. While such a deviation is not unexpected, it has not, to our knowledge, been previously observed.

ACKNOWLEDGEMENTS

We are grateful for useful discussions with R. R. Jones, A. P. Hickman, K. LaGattuta, and F. Robicheaux. This work was supported by the U.S. Department of Energy.

-
- [1] D. S. Belić, Gordon H. Dunn, T. J. Morgan, D. W. Mueller, and C. Timmer, *Phys. Rev. Lett.* **50**, 339 (1983).
 - [2] A. Müller, D. S. Belić, B. D. DePaola, N. Djurić, G. H. Dunn, D. W. Mueller, and C. Timmer, *Phys. Rev. Lett.* **56**, 127 (1986).
 - [3] T. Bartsch *et al.*, *Phys. Rev. Lett.* **79**, 2233 (1997).
 - [4] J. G. Story, B. J. Lyons, and T. F. Gallagher, *Phys. Rev. A* **51**, 2156 (1995).
 - [5] T. F. Gallagher, in *Atomic Excitation and Recombination in External Fields*, edited by M. H. Nayfeh and C. W. Clark (Gordon and Breach, New York, 1985).
 - [6] J. P. Connerade, *Proc. R. Soc. London Ser. A* **362**, 361 (1978).
 - [7] S. A. Bhatti, C. L. Cromer, and W. E. Cooke, *Phys. Rev. A* **24**, 161 (1981).
 - [8] J. G. Story, L. D. Van Woerkom, and W. E. Cooke, *Phys. Rev. A* **34**, 4508 (1986).
 - [9] A. Lindgard and S. E. Nielson, *At. Data Nucl. Data Tables* **19**, 543 (1977).
 - [10] F. Gounand, T. F. Gallagher, W. Sandner, K. A. Safinya, and R. Kachru, *Phys. Rev. A* **27**, 1925 (1983).
 - [11] O. C. Mullins, Y. Zhu, E. Y. Xu, and T. F. Gallagher, *Phys. Rev. A* **32**, 2234 (1985).
 - [12] R. R. Jones and T. F. Gallagher, *Phys. Rev. A* **39**, 4583 (1989).
 - [13] W. E. Cooke, T. F. Gallagher, S. A. Edelstein, and R. M. Hill, *Phys. Rev. Lett.* **40**, 178 (1978).
 - [14] W. E. Cooke and T. F. Gallagher, *Phys. Rev. Lett.* **41**, 1648 (1978).
 - [15] R. Kachru, H. B. van Linden van den Heuvell, and T. F. Gallagher, *Phys. Rev. A* **31**, 700 (1985).
 - [16] N. H. Tran, P. Pillet, R. Kachru, and T. F. Gallagher, *Phys. Rev. A* **29**, 2640 (1984).
 - [17] K. LaGattuta, I. Nasser, and Y. Hahn, *J. Phys. B* **20**, 1565 (1987).
 - [18] K. LaGattuta and Y. Hahn, *Phys. Rev. Lett.* **51**, 558 (1983).
 - [19] K. LaGattuta, I. Nasser, and Y. Hahn, *Phys. Rev. A* **33**, 2782 (1986).
 - [20] C. Bottcher, D. C. Griffin, and M. S. Pindzola, *Phys. Rev. A* **34**, 860 (1986).